The EMBO Journal (2012) 31, 720–730 | © 2012 European Molecular Biology Organization | Some Rights Reserved 0261-4189/12
www.embojournal.org

THE EMBO JOURNAL

EMBO open

Symmetry-free cryo-EM structures of the chaperonin TRiC along its ATPase-driven conformational cycle

Yao Cong[1,4], Gunnar F Schröder[2,5], Anne S Meyer[3,6], Joanita Jakana[1], Boxue Ma[1], Matthew T Dougherty[1], Michael F Schmid[1], Stefanie Reissmann[3,7], Michael Levitt[2], Steven L Ludtke[1], Judith Frydman[3] and Wah Chiu[1,*]

[1]Verna and Marrs McLean Department of Biochemistry and Molecular Biology, National Center for Macromolecular Imaging, Baylor College of Medicine, Houston, TX, USA, [2]Department of Structural Biology, Stanford University, Stanford, CA, USA and [3]Department of Biology and BioX Program, Stanford University, Stanford, CA, USA

The eukaryotic group II chaperonin TRiC/CCT is a 16-subunit complex with eight distinct but similar subunits arranged in two stacked rings. Substrate folding inside the central chamber is triggered by ATP hydrolysis. We present five cryo-EM structures of TRiC in apo and nucleotide-induced states without imposing symmetry during the 3D reconstruction. These structures reveal the intra- and inter-ring subunit interaction pattern changes during the ATPase cycle. In the apo state, the subunit arrangement in each ring is highly asymmetric, whereas all nucleotide-containing states tend to be more symmetrical. We identify and structurally characterize an one-ring closed intermediate induced by ATP hydrolysis wherein the closed TRiC ring exhibits an observable chamber expansion. This likely represents the physiological substrate folding state. Our structural results suggest mechanisms for inter-ring-negative cooperativity, intra-ring-positive cooperativity, and protein-folding chamber closure of TRiC. Intriguingly, these mechanisms are different from other group I and II chaperonins despite their similar architecture.
The EMBO Journal (2012) **31,** 720–730. doi:10.1038/emboj.2011.366; Published online 1 November 2011
Subject Categories: proteins; structural biology
Keywords: asymmetric intermediate; conformational cycle; cryo-EM; protein folding; TRiC/CCT

*Corresponding author. Verna and Marrs McLean Department of Biochemistry and Molecular Biology, National Center for Macromolecular Imaging, Baylor College of Medicine, Houston, TX 77030, USA. Tel.: +1 713 798 6985; Fax: +1 713 798 8682; E-mail: wah@bcm.edu
[4]Present address: Institute of Biochemistry and Cell Biology, Shanghai Institutes for Biological Sciences, Chinese Academy of Sciences, Shanghai 200031, China
[5]Present address: Institute of Complex Systems (ICS-6), Forschungszentrum Jülich, 52425 Jülich, Germany
[6]Present address: Department of Bionanoscience, Kavli Institute of Nanoscience, Delft University of Technology, Lorentzweg 1, 2628 CJ Delft, The Netherlands
[7]Present address: Max-Planck-Institut für Terrestrische Mikrobiologie, Karl-von-Frisch Strasse, 35043 Marburg, Germany

Received: 11 January 2011; accepted: 14 September 2011; published online: 1 November 2011

Introduction

Defects in protein folding are associated with a wide variety of human diseases, including cancer and amyloid diseases such as Huntington's, Parkinson's, and Alzheimer's diseases (Gregersen *et al*, 2000; Dobson, 2004). The eukaryotic chaperonin TRiC/CCT (TCP1-ring complex or chaperonin containing TCP1) folds ~5–10% of newly synthesized cytosolic proteins, including many essential proteins such as actin, tubulin, and cell-cycle regulators (Rommelaere *et al*, 1993; Chen *et al*, 1994; Thulasiraman *et al*, 1999; Spiess *et al*, 2004; Yam *et al*, 2008). The TRiC conformation induced by ATP hydrolysis is closely associated with the productive folding of the substrate (Meyer *et al*, 2003).

Chaperonins have diverged into two structurally and mechanically distinct families: prokaryotic group I chaperonins such as GroEL–GroES from *E. coli* (Xu *et al*, 1997; Bukau and Horwich, 1998) and group II chaperonins, which are further divided into archaeal types (including the thermosome, Ditzel *et al*, 1998; KS-1, Shomura *et al*, 2004; and Mm-cpn, Kusmierczyk and Martin, 2003a, b; Reissmann *et al*, 2007), and the eukaryotic chaperonin TRiC (Frydman *et al*, 1992). Chaperonin subunits share a common architecture, that is, each consists of three domains (apical, intermediate, and equatorial). Unlike GroEL, which employs an additional cofactor (GroES) acting as a detachable lid (Xu *et al*, 1997; Bukau and Horwich, 1998), group II chaperonins have a built-in lid formed by a protrusion at the tip of the apical domain of each individual subunit (Ditzel *et al*, 1998). In addition, GroEL and archaeal chaperonins consist of 1–3 types of subunits, whereas each ring of TRiC contains eight different subunits sharing 27–39% sequence identity (Archibald *et al*, 2001; Cong *et al*, 2010). The hetero-oligomeric nature of TRiC implies an inherently asymmetric arrangement among the subunits; however, little is known about how such structural organization is related to its functional activity. Notably, the eukaryotic TRiC has unique functions that the archaeal chaperonins cannot perform, despite their similar architecture. For instance, many TRiC substrates cannot be folded by any other chaperonin (Tian *et al*, 1995; Frydman, 2001; Hartl and Hayer-Hartl, 2002). This suggests that TRiC must have unique specificity and properties required for maintaining protein homeostasis in the eukaryotic system.

There have been several cryo-EM studies of TRiC in the apo and a variety of nucleotide-containing states (Llorca *et al*, 1999, 2001; Booth *et al*, 2008; Cong *et al*, 2010). The 4 Å cryo-EM structure of the closed state suggested a specific model for the 8-subunit arrangement (Cong *et al*, 2010). Recently, two crystal structures of TRiC bound with tubulin or actin and ATP analogue were reported (Dekker *et al*, 2011; Munoz *et al*, 2011) and suggested an alternative 8-subunit arrangement different from the cryo-EM model. Therefore,

the true ordering of the eight subunits in TRiC complex remains uncertain.

The present investigation is aimed at determining the quaternary structure changes undertaken by TRiC during its ATPase cycle. We report five cryo-EM maps of TRiC in the apo state and the chemically distinct nucleotide-containing states throughout the ATPase cycle. We did not impose symmetry in the 3D reconstruction process, and unlike other group II chaperonins, this study revealed a surprising degree of asymmetry in the conformation of the open, nucleotide-free state. Our composite structures have revealed a distinct interaction pattern of the 16 TRiC subunits in each of these biochemical states, led to a plausible mechanism of lid closure and could illuminate the positive and negative cooperative phenomena occurring in TRiC upon ATP hydrolysis.

Results

Cryo-EM maps of TRiC throughout the ATPase cycle

To investigate the structural mechanisms of TRiC conformational transitions during its ATPase cycle (Figure 1), we carried out single particle cryo-EM studies of bovine TRiC in well-defined biochemical states: apo (nucleotide-free), ATP-bound (mimicked by non-hydrolysable ATP analogue AMP-PNP), ADP-bound, and two ATP-hydrolysis transition state analogues induced by ADP-AlFx and ATP-AlFx, respectively (Meyer *et al*, 2003). Each nucleotide state was obtained by incubation of TRiC with the respective nucleotide analogue and buffer (see Materials and methods).

As the first step of the analysis, we carried out reference-free 2D image analysis on the end-on view images to evaluate

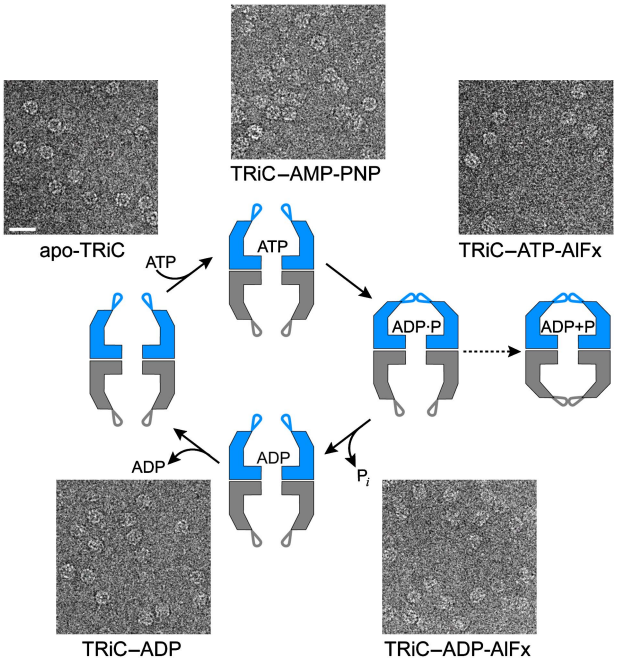

Figure 1 Cryo-EM study of TRiC conformational cycle. Cartoon diagram illustrates the TRiC conformational transitions in the apo state and four distinct nucleotide biochemical states throughout the ATPase cycle. In addition, a representative micrograph of ice-embedded TRiC in each state is shown. Scale bar is 320 Å.

whether there is any obvious conformational heterogeneity in each state. TRiC–ADP-AlFx showed two drastically different 2D image patterns, suggesting structural heterogeneity. One has the characteristic appearance of a both-ring open conformation (Supplementary Figure S1A) while the other shows a unique twisted pattern of all the subunits (Supplementary Figure S1B). The 2D images of the other states appeared more homogeneous. Therefore, a multi-reference refinement procedure in EMAN1 (Chen *et al*, 2006) was adopted for the TRiC–ADP-AlFx data set, while the standard refinement procedure was applied to the other states.

Since the eight subunits of TRiC are all different, no symmetry was imposed in the reconstruction process for all the five states presented here (Figures 2 and 3), allowing us to assess structural differences among the eight distinct subunits. The closed ATP-AlFx state was previously determined at 4.7 Å resolution (Cong *et al*, 2010), while the resolutions of the other four states were found to be 10.5–13.9 Å (Supplementary Figure S2). This resolution limit can be attributed to preferred particle orientation on the cryo-EM grid, continuous conformational variations, and/or subtle structural heterogeneity in TRiC, which have been found in cryo-EM studies of group II chaperonins (Clare *et al*, 2008; Zhang *et al*, 2011).

A unique asymmetric pattern among the eight subunits of TRiC in the nucleotide-free state

The end-on view of apo-TRiC reveals an obvious asymmetric pattern among its eight distinct subunits (Figure 2A). However, we cannot determine the subunit identity in this map determined at 10.5 Å resolution. Nevertheless, the structural features of the subunits are distinct enough to annotate them from a_1 to a_8 for one ring and a'_1 to a'_8 for the other ring. A cylindrical 'unwrapping' was applied to the map, and exhibits a pseudo two-fold symmetry between the two rings (Figure 4A). This symmetry was confirmed quantitatively by the rotational correlation analysis between the two rings (Figure 5A). This pseudo two-fold symmetry is located at the inter-ring interfaces between subunits a_1 and a'_1, and a_5 and a'_5 (Figure 2A). Therefore, both of the densities (a_1 and a'_1) should correspond to the same CCT subunit; and the same applies to a_5 and a'_5. The presence of the pseudo two-fold axis in this symmetry-free reconstruction reinforces our previous observation in the 4.7 Å resolution cryo-EM structure of TRiC–ATP-AlFx (Cong *et al*, 2010). Therefore, the subunit ordering is identical in both rings but arranged in opposite directions as viewed from the side (Figure 4A). Since the question of subunit ordering of TRiC still remains uncertain (Cong *et al*, 2010; Dekker *et al*, 2011), we will only refer to the subunits in the complex as a_1–a_8. Our conclusions are valid for both proposed models, since both agree on the existence of an inter-ring two-fold symmetry axis.

In the apo-TRiC map, both a_1 and a'_1 subunits display a significantly weaker density than all the other subunits (Figure 4A). This structural characteristic may be caused by the extremely dynamic nature of this subunit as shown in a movie generated from a superposition of a set of reference-free 2D averages of end-on views (Supplementary Movie 1A). Such subunit flexibility is analogous to a large crystallographic B-factor, making a high-resolution structural

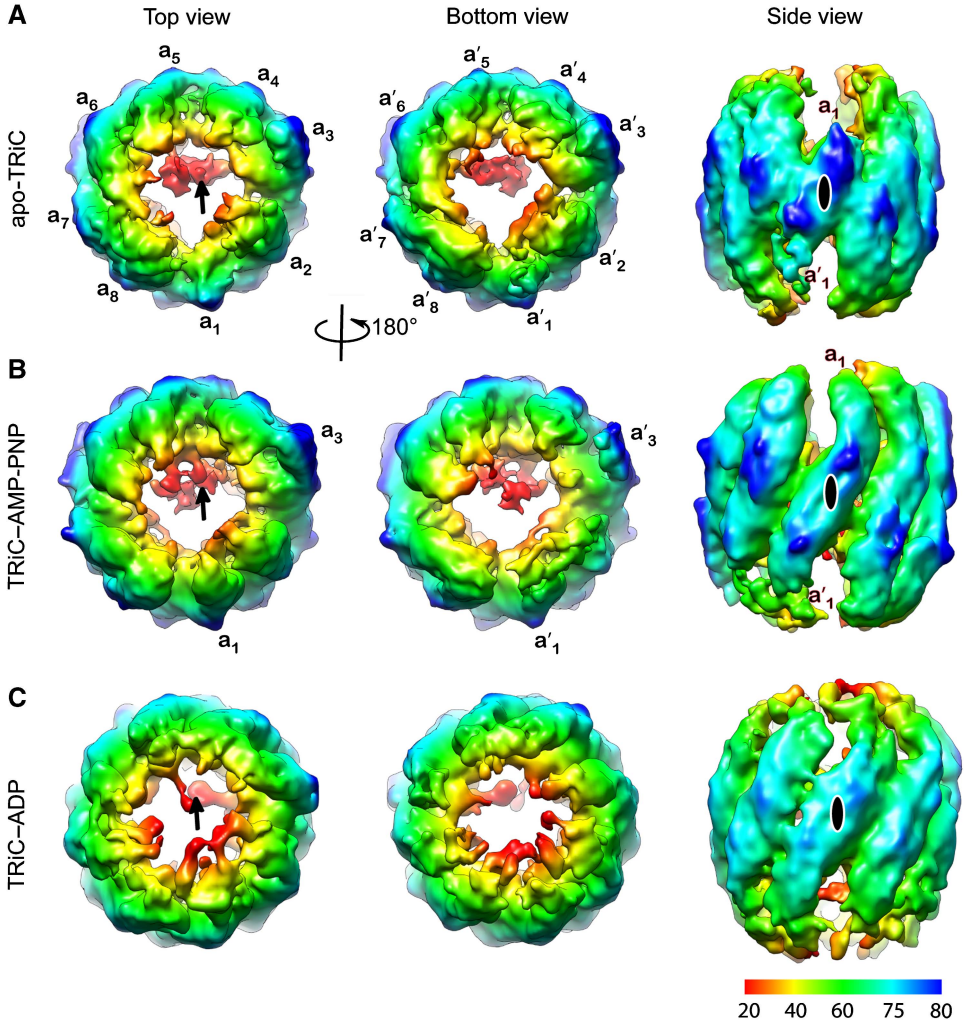

Figure 2 Symmetry-free cryo-EM maps of TRiC in the three open conformational states. (**A**) Top, bottom, and side views of apo-TRiC. In the top ring, the subunits were labelled as a_1–a_8; whereas in the bottom ring, the subunits were labelled as a'_1–a'_8. The location of the pseudo two-fold axis was labelled in the side view. The extra density seen in the equatorial domain region is indicated by a black arrow. (**B**) Equivalent views of TRiC–AMP-PNP (ATP-bound state). (**C**) Equivalent views of TRiC–ADP (ADP-bound state). The same radial colour scheme from the centre of a cylinder is used throughout.

determination of the apo state impractical (Zhang *et al*, 2010). Contrary to a_1 and a'_1, the densities of both a_5 and a'_5 are better resolved in both rings, and thus more rigid (Supplementary Movie 1A; Figure 2A).

Another characteristic subunit in this apo-TRiC map is a_3, which appears to tilt outward from the central chamber (Figure 5B) and lean towards one of its neighbouring subunits (a_4), thus separating it further from the other neighbouring subunit (a_2) (Figures 4A and 5B). The unwrapped displays (Figure 4) show the relationship between the subunit pairs across the rings, for instance, a_3–a'_7, a_4–a'_6 etc. Figure 4A shows that the line between subunit a_3 in one ring and subunit a'_7 in the other ring has a larger tilt angle and is less parallel (Figure 4A) to the lines joining other subunit pairs (e.g., a_2 and a'_8).

Based on the above observations, it is tempting to postulate that the conformations of the very dynamic subunit (a_1) and/or the outward tilting one (a_3) might make them more likely to encounter the substrate proteins in solution and be critical for substrate recruiting of TRiC.

The TRiC lid remains open in three states of the cycle: ATP bound, ADP bound, and nucleotide free

The distinct open conformational states of TRiC occur at essential steps during the folding cycle and facilitate the binding of substrate proteins (Meyer *et al*, 2003; Reissmann *et al*, 2007). Here, our maps in the apo, ATP-, and ADP-bound states reveal that the apical domains of TRiC generally extend towards the central chamber in different angles with a slight upward tilt (Figure 2; Supplementary Figure S3A–C). Importantly, akin to the apo and ADP-bound states (Figure 2A and C), our maps clearly demonstrate that TRiC remains open in the ATP-bound state (TRiC–AMP-PNP; Figure 2B). This is consistent with previous biochemical and biophysical studies of TRiC (Szpikowska *et al*, 1998; Gutsche *et al*, 2000; Meyer *et al*, 2003; Reissmann *et al*, 2007) and recent structural studies on group II chaperonins (Huo *et al*, 2010; Douglas *et al*, 2011; Munoz *et al*, 2011; Zhang *et al*, 2011). Thus, our observations unambiguously show that nucleotide binding alone is not sufficient to trigger lid closure.

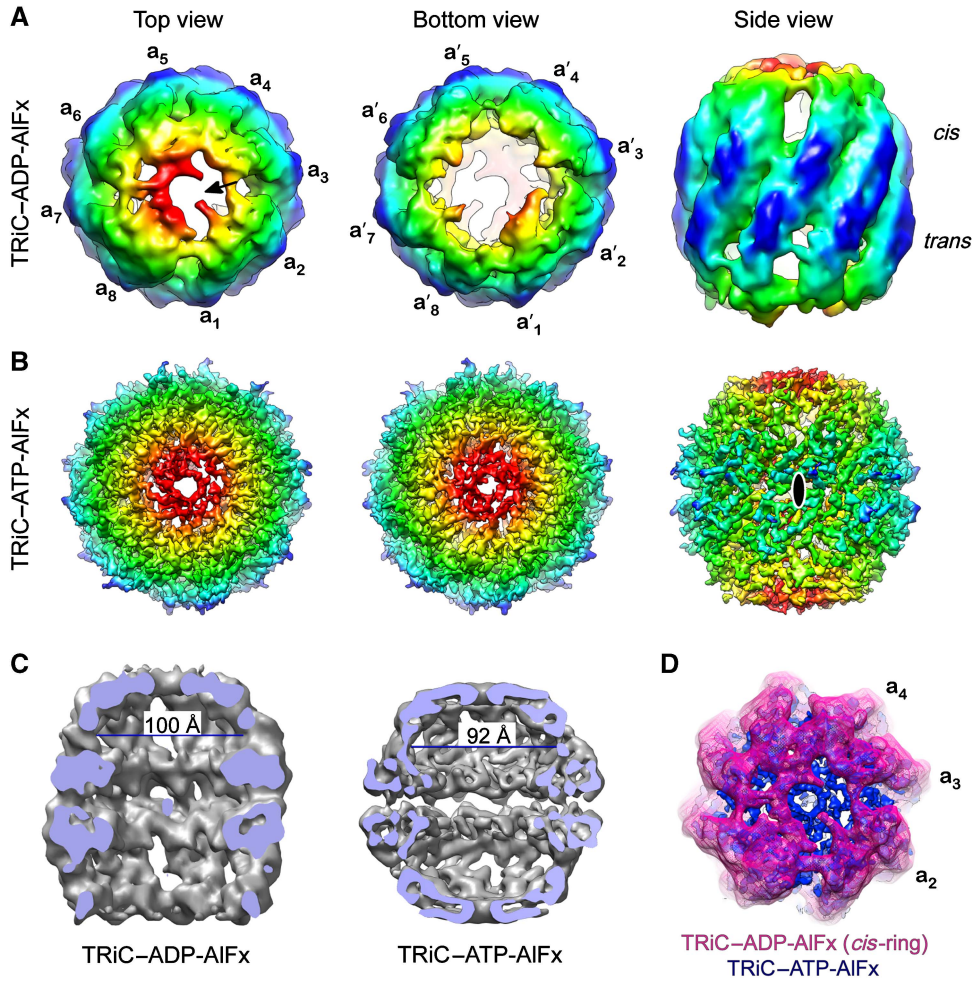

Figure 3 Symmetry-free cryo-EM density maps of TRiC in the ADP-AlFx and ATP-AlFx states. The same colour scheme is adopted as in Figure 2. (**A**) Top, bottom, and side views of TRiC–ADP-AlFx in an asymmetric conformation with the *cis*-ring closed while the *trans*-ring still open. There is a small opening in the lid around subunits a_3 (indicated by a black arrow). (**B**) Views of TRiC–ATP-AlFx in a both ring closed conformation (Cong *et al*, 2010). (**C**) TRiC–ADP-AlFx closed *cis*-ring chamber inter-volume diameter (~100 Å) compared with that of TRiC–ATP-AlFx (~92 Å). The diameter was measured at the equivalent location of the intermediate domain of the two rotational averaged maps. The high-resolution TRiC–ATP-AlFx map was blurred to ~10 Å, in a comparable manner to the ADP-AlFx map. (**D**) Overlapping of the closed ring of TRiC–ADP-AlFx (in purple) and TRiC–ATP-AlFx (in dark blue) showing different extents of TRiC chamber closure, that is, the closed ring in TRiC–ATP-AlFx is more compact than that in TRiC–ADP-AlFx.

Structural variations induced by nucleotide binding

Upon nucleotide binding (AMP-PNP or ADP state), TRiC remains open in both rings similar to the apo state (Figure 2), and a pseudo two-fold symmetry between two rings persists in these conformational states (Supplementary Figure S4). Strikingly, after nucleotide binding the densities of subunits a_1 and a'_1 appear to be better defined based on the 2D end-on view image analysis (Supplementary Movie 1B and C), and the entire complex appears slightly more symmetrical in 3D (Supplementary Movie 2). These observations are confirmed by the 3D reconstructions, for instance, the missing density corresponding to subunits a_1 and a'_1 in apo-TRiC is restored in the AMP-PNP and ADP states (Figure 4B and D). Of note, the TRiC–AMP-PNP map demonstrates that the apical domain of subunit a'_1 in the bottom ring is less well resolved than its counterpart a_1 in the top ring (Figure 4B). This finding indicates that a_1 is possibly better poised than a'_1 for the lid closure of the top ring, which might require all the subunits in one ring to be more symmetrically arranged. Such asymmetry between a_1 and a'_1 may reflect the negative inter-ring cooperativity of TRiC (Kafri *et al*, 2001; Reissmann *et al*, 2007).

In total, our data reveal that nucleotide binding can cause the subunit to be more rigid and the arrangement to become more symmetric while still open. However, nucleotide binding is not sufficient to close the folding chamber. This mechanism is in strong contrast to group I chaperonins such as GroEL, which undergo their major conformational rearrangement upon binding, not upon hydrolysis of ATP (Xu *et al*, 1997). This difference could be related to the fact that GroEL has a detachable lid (GroES) to cover the chamber, while TRiC instead has a built-in lid. Hence, the energy needed for chamber closure might be different.

Interestingly, the outward tilt of the subunits a_3 and a'_3 in the apo state is preserved upon nucleotide binding, as seen in the AMP-PNP state (Figure 5C and F; Supplementary Movie 2). This outward tilting subunit is also seen in the crystal structure of TRiC–ATP-γ-S in complex with tubulin (2XSM) (Munoz *et al*, 2011). This ATP-bound state (ATP-γ-S) is equivalent to our AMP-PNP state. These two structures

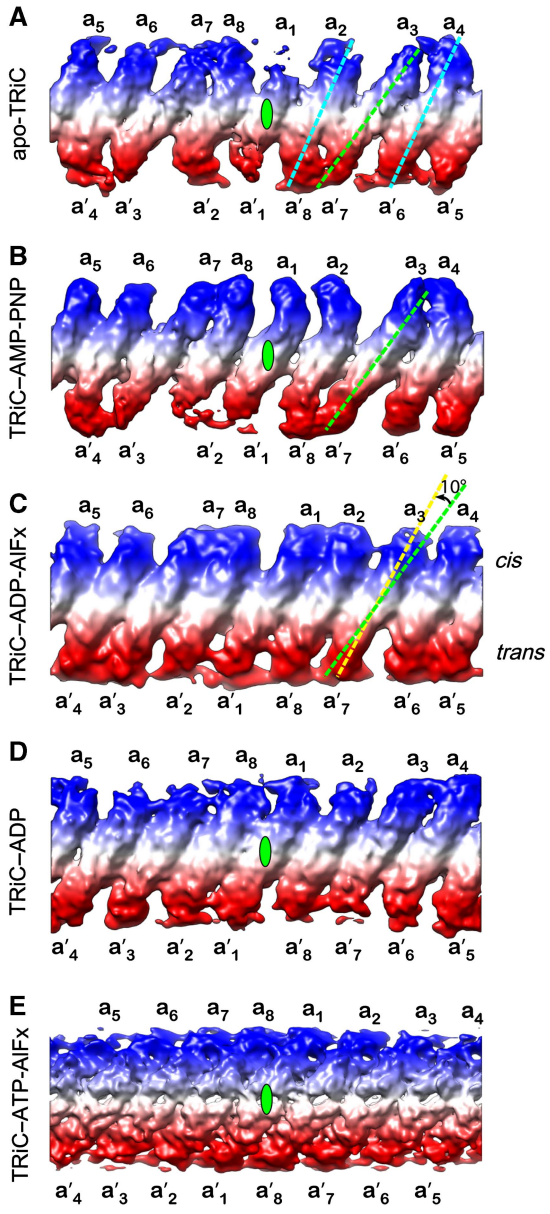

Figure 4 Unwrapped maps of TRiC in different biochemical states. By cutting the map and unrolling it onto a planar surface, we can see all of the subunits and their positional relationships more clearly. (**A**) Side view of the apo-TRiC unwrapped map, visualized from outside of the complex. The upper ring subunits are rendered in blue and the lower ring subunits in red, while the interacting equatorial domain regions in both rings are white. The location of the pseudo two-fold axis is labelled as a green ellipsoid. The top ring subunits are labelled as a_1–a_8, while the bottom ring subunits labelled as a'_1–a'_8. The tilt angle of the characteristic subunits a_3 and its connecting subunit a'_7 is highlighted with a green dotted line, as a comparison the tilt angles of subunit pairs a_2–a'_8 and a_4–a'_6 are also labelled (cyan dotted lines). (**B**) Side view of the unwrapped map of TRiC–AMP-PNP. The tilt angle of the characteristic subunits pair a_3–a'_7 is comparable to that in apo-TRiC and still highlighted with a green dotted line. A similar rendering style as in (**A**) was adopted hereafter. (**C**) Side view of the unwrapped map of TRiC–ADP-AlFx, with *cis*-ring (upper) in blue and *trans*-ring (lower) in red. The tilt angle of subunit pair a_3–a'_7 is labelled in yellow dotted line, which is reduced $\sim 10^\circ$ as compared with that in the AMP-PNP state (green dotted line). (**D**, **E**) Side view of the unwrapped map of TRiC–ADP/TRiC–ATP-AlFx. To render the features of the maps in a comparable manner, the high-resolution TRiC–ATP-AlFx map was blurred into a similar resolution as the other maps. In the unwrapping process, due to oversampling in the region close to the cylindrical axis, there might be slight distortions in the unwrapped map especially in the inward tilting upper apical domain regions, similar to a Mercator Projection of a global map of the Earth.

match well (Supplementary Figure S5), providing strong evidence for the existence of this unique conformation of TRiC in the ATPase cycle.

All open states display an extra density in the equatorial domain inside the chamber around subunit a_6 in one ring and around subunit a'_7 in the other ring (indicated by the black arrow in Figure 2). These densities may correspond to the C and N termini (Supplementary Figure S6A), which have also been observed in the 4.7 Å resolution TRiC–ATP-AlFx map (Cong *et al*, 2010; Supplementary Figure S6B).

The characteristic outward tilt of subunits a_3 and a'_3, the location of the pseudo two-fold symmetry axis, and the extra density in the equatorial domain allowed us to put the structures of these three states in register. Both the self-correlation function for each map (Supplementary Figure S7) and the 2D end-on view movie (Supplementary Movie 1) reveal that the ADP state (Figure 4D), which is the end state of the ATP-hydrolysis cycle and might be the substrate acceptor state, appears to be slightly more symmetrical than the other two states (Figure 4A and B).

An asymmetrically closed conformation of TRiC in the ATP hydrolysis transition state

TRiC–ADP-AlFx, the trigonal-bipyramidal ATP hydrolysis transition state (Melki *et al*, 1997), has been demonstrated to represent the physiological substrate folding state (Kafri *et al*, 2001; Kafri and Horovitz, 2003; Meyer *et al*, 2003; Reissmann *et al*, 2007; Douglas *et al*, 2011). This biochemical state contains a mixture of two TRiC conformations (Supplementary Figure S1A and B). In all, 35% of the data were classified into a conformation with both rings open (Supplementary Figure S1C). The map generated from the remaining data displays an asymmetric conformation with one ring closed (*cis*-ring) and the other ring open (*trans*-ring) (Figures 3A and 5D). Using the correlation between this asymmetric TRiC–ADP-AlFx map and the TRiC–AMP-PNP map (Figure 5E), we can register their subunits in both rings (Figure 5G and H). This registration is also apparent in the match of the characteristic outward tilting subunits a_3 and a'_3 in the two maps (Figure 5G and H).

In the closed *cis*-ring, we observe a collective inward tilt motion of all eight subunits (Figure 6A; Supplementary Movie 3) and a more symmetrical arrangement relative to all the open states (Figures 2, 3A, and 5G). The apical domain protruding densities from each subunit come together and have more contacts to form a lid covering the central chamber of the *cis*-ring. Although the characteristic subunit a_3 tilts inwards slightly, it displays relatively less contact with its neighbouring a_2 subunit (Figure 5G) and leaves a small opening in the covering lid at the rendering threshold (indicated by black arrow in Figure 3A, and also shown in Figure 3D). Conversely, the apical protruding density of a_3 is closer to subunit a_4. It is not known if such an arrangement exists in the presence of substrate. If it does, a productive

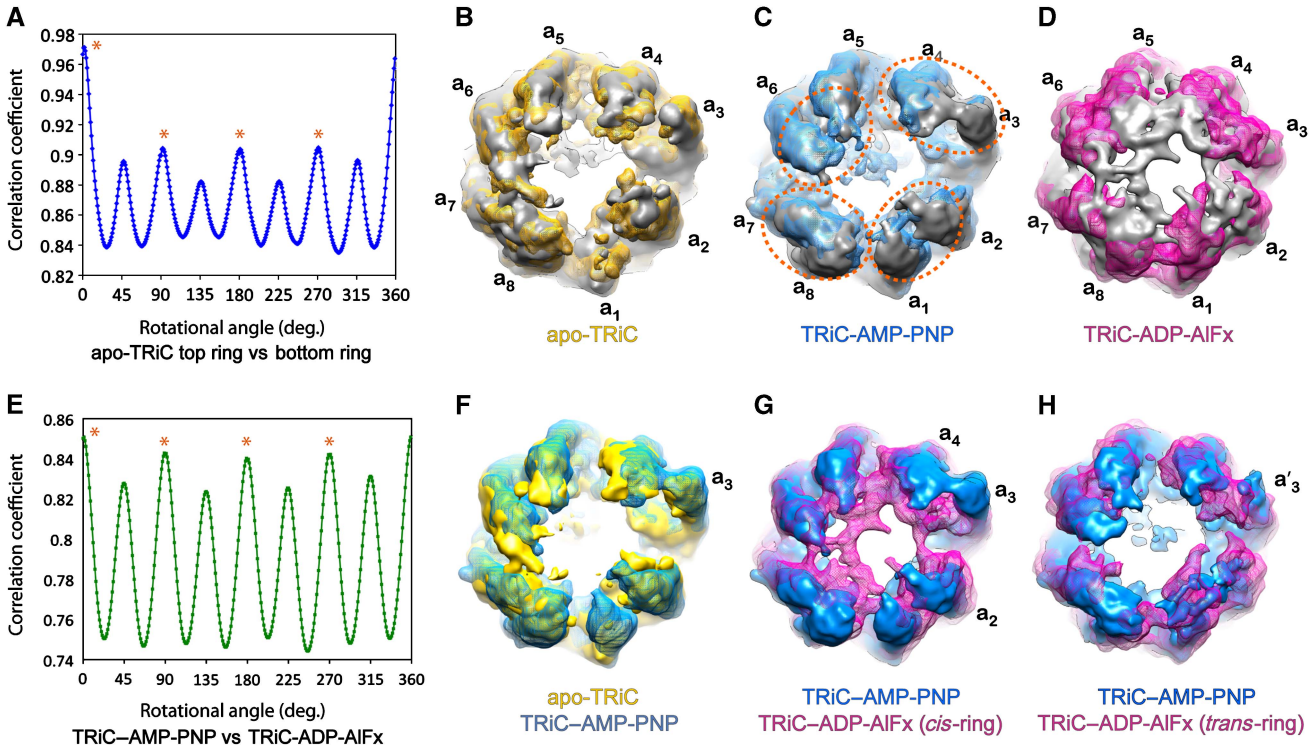

Figure 5 TRiC conformational comparison and transition in the ATPase cycle. (**A**) Rotational correlation analysis between the two rings of apo-TRiC, with the top ring fixed and bottom ring rotated. At 0°, the two rings have the best correlation score, indicating the location of the two-fold axis as illustrated in Figure 2A. Among the eight peaks, four of them have higher value and were highlighted by orange stars indicating the existence of a pseudo four-fold symmetry in the complex. (**B**) Conformational comparison between the two rings of apo-TRiC (top ring in grey and bottom ring in yellow). (**C**) Conformational comparison between the two rings of TRiC–AMP-PNP (top ring in grey and bottom ring in cyan). (**D**) Conformational variation between the two rings of TRiC–ADP-AlFx (*cis*-ring in grey and *trans*-ring in purple). (**E**) Rotational correlation analysis between TRiC–AMP-PNP and TRiC–ADP-AlFx. At 0°, the two maps have the best correlation score, indicating the best alignment angle between the two maps as illustrated in (**G**, **H**). As in (**A**), among the eight peaks, four of them have higher value and were labelled by orange stars. (**F**) Conformational variation between apo-TRiC (in yellow) and TRiC–AMP-PNP (in cyan). (**G**, **H**) Conformational transition from the ATP-bound state to the ATP hydrolysis transition state with (**G**) showing the closed *cis*-ring of TRiC–ADP-AlFx overlaid with the open top ring of TRiC–AMP-PNP, and (**H**) showing the open *trans*-ring of TRiC–ADP-AlFx aligned with the other open ring of TRiC–AMP-PNP.

folding of a substrate inside the chamber may not require a complete closure of the lid.

Expansion of the folding chambers in the ATP hydrolysis transition state

Careful comparison of the closed *cis*-ring of TRiC–ADP-AlFx with the closed ring of TRiC–ATP-AlFx reveals that on average the chamber of the *cis*-ring of TRiC–ADP-AlFx is slightly wider (~8 Å) than that of the other state (Figure 3C and D). This expansion results in a volume of ~180 000 Å^3 for the closed folding chamber. It has been suggested that group II chaperonins can assist folding of proteins around 40–70 kDa (Spiess *et al*, 2004; Yam *et al*, 2008). Such chamber size in TRiC is comparable to that of the closed *cis*-ring of GroEL–GroES (~175 000 Å^3), which can accommodate substrates up to 70 kDa (Xu *et al*, 1997).

The subunits in the open *trans*-ring of TRiC–ADP-AlFx exhibit a visible outward tilt motion of the intermediate and apical domains as compared with the AMP-PNP state (Figure 6A). This motion leads to a noticeable chamber enlargement of the *trans*-ring (Figure 6A), which would be the physiological acceptor state for the next round of substrate and nucleotide binding.

ATP hydrolysis enhances the intra-ring TRiC subunit interactions

Our cryo-EM maps of TRiC in multiple nucleotide states depict different intra-ring subunit interaction patterns throughout the ATPase cycle. In the open states, the maps reveal contacts among the apical domain in some but not all of the neighbouring subunits (Figure 5B and C). The eight subunits in each ring appear to group into four subunit pairs (a_1–a_2, a_3–a_4, a_5–a_6, and a_7–a_8) that create a pseudo four-fold symmetry in TRiC, whereby each ring would be formed by a tetramer of dimers. This can be clearly observed especially in the map of TRiC–AMP-PNP (Figure 5C). This pattern of four subunit pairs within a ring might be related to the differential ATP binding and hydrolysis rate among different TRiC subunits (Reissmann, 2007). Upon ATP hydrolysis, the apical-domain interactions among all subunits become more extensive in the closed *cis*-ring (Figure 3A) and result in shutting the *cis*-ring chamber (Figure 3A and D).

As for TRiC–ATP-AlFx, a similar intra-ring contacting pattern to that in the *cis*-ring of TRiC–ADP-AlFx was detected (Figure 3B and D). Interestingly, our map also reveals additional contacts between the apical/intermediate domain of some subunits and its neighbouring equatorial domain, similar to that in the closed thermosome structure (Ditzel *et al*,

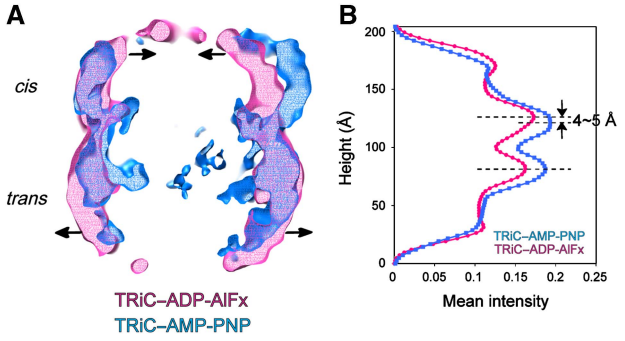

Figure 6 The structural mechanism of TRiC negative inter-ring cooperativity. (**A**) Conformational comparison between TRiC–AMP-PNP (in light blue) and TRiC–ADP-AlFx (in purple). Only the side view of a central slide of the two maps was shown. The direction of the inward/outward tilt motion in the *cis*- and *trans*-rings of TRiC–ADP-AlFx is indicated by black arrows. (**B**) The plot of the density map mean intensity versus the height of TRiC. The plot for TRiC–AMP-PNP is in light blue, and that for TRiC–ADP-AlFx in purple. The top two ranking peaks (indicated by dotted lines) correspond to the location of the most condensed region in the equatorial domain in each ring. There is a detectable distance enlargement (4–5 Å) between the two rings of TRiC induced by ATP hydrolysis.

1998). These extra interactions formed in TRiC–ATP-AlFx might be the potential forces making its chamber more compact and even more symmetrical than that of the *cis*-ring of TRiC–ADP-AlFx (Figures 3B, D, and 4E). In summary, the apical-domain interaction is maintained or enhanced throughout the ATPase cycle, which suggests its key role in maintaining the association and communication of the TRiC subunits within one ring.

Discussion

Chamber closing mechanisms of TRiC

A number of efforts have been made to describe the mechanism of TRiC chamber closure based on cryo-EM studies (Llorca *et al*, 1999, 2001; Booth *et al*, 2008). However, this issue remains uncertain because (a) eight-fold symmetry was imposed in their reconstructions and (b) none of these studies included multiple intermediate states. In the present study, we obtained symmetry-free maps of TRiC for four nucleotide-containing states in addition to the apo state. The asymmetrically closed intermediate (TRiC–ADP-AlFx), especially, representing the key physiological substrate folding state, is structurally determined for the first time.

By not imposing symmetry, we uncovered structural details not previously seen in group II chaperonins (Xu *et al*, 1997; Llorca *et al*, 1999, 2001; Booth *et al*, 2008; Clare *et al*, 2008; Pereira *et al*, 2010; Zhang *et al*, 2010). Our analysis clearly shows that the ATP hydrolysis-induced chamber closure motion for each of the subunits is different (Figure 5G; Supplementary Movie 3). A comparison of the subunit arrangement in Figure 4A–E shows a trend of increasing pseudo symmetry during the ATP hydrolysis cycle. The most characteristic and dramatic change is found in the a_3–a'_7 subunit pair. They may possibly play a critical role in initiating the formation of pseudo symmetry by increasing the extent of apical-domain interactions among all the subunits of that ring. This symmetry would lead to positive cooperativity among subunits in one ring and result in chamber closure of the *cis*-ring.

Though the motion of each subunit is unique (Supplementary Movie 3), the overall ATP hydrolysis-induced chamber closure motion is similar for each subunit. To demonstrate the motion (Supplementary Movie 4), we use the subunit a_5 and a'_5 pair as an example, which appear to have minimum motion among the subunits. The *cis*-ring subunits move 'upwards' (towards the top of the barrel), and each domain of each subunit tilts inwards with slightly different motions. In the *trans*-ring subunits, the apical domains move neither downwards nor inwards. Rather, in some of the *trans*-ring subunits, the apical and intermediate domains tilt outwards (Figure 6A); while the equatorial domains of most *trans*-ring subunits move radially outward slightly. This outwards motion could prevent the closure of the *trans*-ring. This opposing motion is a plausible indication of the negative cooperativity of the two rings.

Mechanism of TRiC negative inter-ring cooperativity

Our characterization of the one-ring closed intermediate TRiC–ADP-AlFx provides some unexpected insights into the structural basis of its negative inter-ring cooperativity. ATP hydrolysis causes a spatial rearrangement at the interface between the two rings, as in the case of GroEL (Xu *et al*, 1997; Ma *et al*, 2000). This rearrangement results in an observable increase in separation between the rings in TRiC–ADP-AlFx (Figure 6B; Supplementary Movie 4), while the two major inter-ring contacts are maintained, as in all group II chaperonins (Ditzel *et al*, 1998). Such a distance increase could reduce the buried surface between the two rings and potentially modify the salt bridges formed between certain opposing subunit pairs (Ditzel *et al*, 1998), which will vary the interaction network between the rings.

Closely related to the above-discussed subunit a_3 and a'_7 pair (Figure 4B), our open-state maps reveal that in general if two neighbouring subunits in one ring have formed a pair with contact in the apical domain (e.g., a_3 and a_4), their connected subunits in the other ring (a'_7 and a'_6, respectively) tend to be separated in the apical region (Figure 4A and B). This pattern has not been previously observed, and may play a part in both intra- and inter-ring subunit interactions. Such interactions could contribute to the inter-ring negative cooperativity, making TRiC work as a two-stroke molecular machine. This more complex mechanism of inter-ring negative cooperativity of TRiC compared with GroEL is likely related to their different inter-ring interaction patterns, that is, the interactions are registered in TRiC and other group II chaperonins, while it is staggered in GroEL.

The intra-ring interaction pattern differs among chaperonins

Our structures of TRiC reported here show different intra-ring interaction patterns from its archaeal homologue Mm-cpn or prokaryotic homologue GroEL. In the apo state, all these chaperonins share a common neighbouring equatorial-domain interaction within one ring. However, the interactions between the other domains of adjacent subunits vary substantially. In apo-TRiC, we identified apical-domain interactions between pairs of subunits in the same ring (Figures 2A and 4A). Apo-GroEL contains interactions between adjacent apical domains and has contacts between apical and intermediate domains of neighbouring subunits (Supplementary Figure S8A; Braig *et al*, 1994; Ludtke *et al*,

2008). In contrast, apo-Mm-cpn has no apical- or intermediate-domain contact in the open state, based on the available symmetric structures (Clare *et al*, 2008; Pereira *et al*, 2010; Zhang *et al*, 2010; Supplementary Figure S8B). This is consistent with the report that the intra-ring cooperativity is relatively weak in archaeal chaperonins, and in the *T. acidophilum* thermosome it appears to be absent (Bigotti and Clarke, 2005).

These three chaperonins have thus each evolved a different pattern of intra-ring interactions, indicating that the intrinsic inter-subunit coordination strategy is different among them. The enhanced intra-ring subunit contacts seen in TRiC as compared with Mm-cpn may play an important role in stabilizing and specifying the correct assembly of the eight distinct subunits of TRiC; this could also promote a coordinated rotation between the apical and intermediate domains, beneficial for the lid formation from the eight different subunits in TRiC.

Diverse chamber closing mechanisms among chaperonins might be related to their different intra- and inter-ring interaction patterns

The diverse pattern of intra-ring interactions among the open states of TRiC, Mm-cpn, and GroEL (Supplementary Figure S8; Figure 2; Clare *et al*, 2008; Pereira *et al*, 2010; Zhang *et al*, 2010) suggests that different starting points in the chamber closing process lead to differing trajectories of chamber closure. For apo-Mm-cpn, chamber closure appears to involve primarily rigid-body motion of the entire subunit when comparing only two states (Pereira *et al*, 2010; Zhang *et al*, 2010) and shows some interdomain movements within a subunit when an additional intermediate state is seen (Zhang *et al*, 2011). In both TRiC and GroEL, however, the allosteric rearrangement of their lid closure involves relative domain motion within each subunit. However, the direction of the domain motion is different: in TRiC, the apical and intermediate domains move mostly in the same direction (e.g., in subunits a_1 and a_3, Supplementary Movie 3), while those of GroEL move in the opposite directions (Xu *et al*, 1997; Booth *et al*, 2008). In addition, our study depicts a complex inter-ring subunit co-operativity in TRiC (Figure 4), and cross talk between its intra- and inter-ring allosteric networks which may facilitate its chamber closure. Together, the structural mechanism differences in chamber closure among different chaperonins are related to their differences in intra- and inter-ring subunit interaction pattern, with pronounced differences seen in the open conformations.

This study demonstrates how evolution uses a common structural framework but adopts different mechanical switches due to specific gene sequences and consequent allosteric networks. Furthermore, it is possible that the ATPase cycle of chaperonins might be customized to the unique intracellular environments of various organisms or physiological states by interaction with co-chaperones, substrate proteins and perhaps by distinct post-translational modifications (Southworth and Agard, 2008; Tsutsumi *et al*, 2009).

Materials and methods

Purification of TRiC

TRiC was purified from bovine testis essentially as described (Ferreyra and Frydman, 2000; Feldman *et al*, 2003). In brief, the tubules of bovine testis (500 g) separated from the tunica albuginea by dissection were homogenized in buffer H (20 mM HEPES/KOH (pH 7.4), 5 mM $MgCl_2$, 0.1 mM EDTA, 50 mM NaCl, 1 mM DTT) containing the protease inhibitors leupeptine (2 μg/ml), aprotinin (0.5 μg/ml), pepstatin (0.5 μg/ml) and PMSF (0.2 mM), and the lysate was clarified by centrifugation for 30 min at 20 000 *g* followed by a 1-h centrifugation step at 100 000 *g*. The lysate was subjected to a 35% ammonium sulphate cut, and the resulting supernatant was precipitated with a final concentration of 50% ammonium sulphate. The pellet was resuspended in a small volume of MQ-A buffer (20 mM HEPES/KOH (pH 7.4), 5 mM $MgCl_2$, 0.1 mM EDTA, 50 mM NaCl, 10% glycerol, 1 mM DTT) and 30 ml aliquots, respectively, were loaded on sucrose cushions (lower layer: 2 ml 60% sucrose in MQ-A buffer; upper layer 5 ml 20% sucrose in MQ-A buffer). After 20 h ultracentrifugation in a SW-28 rotor at 26 000 r.p.m. and 4°C, the sucrose cushions together with all sedimented materials were pooled, dialysed against MQ-A buffer, and loaded on a Q Sepharose FF column (60 ml, GE Healthcare, USA) equilibrated in MQ-A buffer. Bound proteins were eluted with 0.4 M NaCl in MQ-A buffer. Fractions containing proteins were pooled and diluted 1:1 in MQ-A buffer before they were loaded on a High-Trap Heparin column (20 ml, GE Healthcare, USA) equilibrated in MQ-A buffer containing 0.2 M NaCl. Bound proteins were eluted by a NaCl gradient ranging from 0.2 to 1 M NaCl. Fractions containing TRiC were pooled, concentrated using an Amicon Ultra-15 10K concentrator (Millipore Corporation, USA), and loaded on a Superose 6 10/300 GL column (GE Healthcare). Fractions containing the oligomeric chaperonin were pooled, and aliquots were flash frozen in liquid nitrogen.

Electron cryo-microscopy

TRiC samples were prepared for cryo-EM studies by dilution of purified TRiC to 0.5 mg/ml. The TRiC sample was proven to be folding active under our freezing conditions by an actin refolding assay (Meyer *et al*, 2003). Nucleotide-free samples were frozen immediately. TRiC–ATP-AlFx/TRiC–ADP-AlFx samples were incubated in the presence of 1 mM ATP/ADP, 5 mM $MgCl_2$, 5 mM $Al(NO_3)_3$, and 30 mM NaF for 1 h at 30°C prior to freezing. For TRiC–ADP/TRiC–AMP-PNP, the sample was incubated in the presence of 1 mM ADP/10 mM AMP-PNP and 5 mM/15 mM $MgCl_2$ for 15 min at 30°C prior to freezing. Since commercial AMP-PNP typically contains impurities (Meyer *et al*, 2003), we performed purification on it by anion exchange chromatography as described (Horst *et al*, 1996). In all, 3 μl of sample was deposited onto a glow-discharged 400/200 mesh Quantifoil holy carbon grid (1.2×1.3 μm hole size, Quantifoil Micro Tools GmbH, Jena Germany). The grid was flash frozen in liquid ethane using a Vitrobot (FEI, Hillsboro, OR, USA). Data were recorded on a JEM 3200FSC microscope (JEOL, Tokyo) equipped with a field-emission gun operated at 300 kV and an in-column energy filter (using 20 eV slit). The spot size was set to 1; the condenser and objective aperture were set to 50 and 120 μm, respectively. Specimen temperature was maintained at 101 K. Images were recorded at $\times 50\,000$ microscope magnification on Kodak SO-163 films with the specimen dose of 18 electrons/Å^2. The images were digitized on a Nikon Super CoolScan 9000 ED scanner with 6.35 μm/pixel scanning interval.

Image processing, 3D reconstruction, and segmentation

The particles were boxed out from digitized micrographs by *boxer* from EMAN 1.8 (Ludtke *et al*, 1999, 2001) and *e2boxer.py* from EMAN2 (Tang *et al*, 2007). CTF parameter estimation was carried out using the EMAN1 program *ctfit*. Reference-free 2D analysis was carried out using *refine2d* program in EMAN1 (Ludtke *et al*, 1999, 2001). For the ADP-AlFx state, there are two conformational states that coexist based on the 2D image analysis (Supplementary Figure S1A), so that *multirefine* procedure in EMAN1 as described previously (Chen *et al*, 2006; Booth *et al*, 2008) was employed. All the 3D reconstructions using EMAN1 were completed with no symmetry imposed. In addition, a recently developed 2D fast rotational matching (FRM2D) algorithm (Cong *et al*, 2003, 2005; Cong and Ludtke, 2010), available in EMAN 1.8+, was adopted in the final refinement. This method has been used to obtain a number of subnanometer resolution cryo-EM maps (Cong *et al*, 2009, 2010). Micrographs with a defocus range of ~1.2–3.5 μm were used in the final reconstruction process. For each of the five states, the particle number included in the final 3D reconstruction was listed in Supplementary Figure S2A. Except for the closed ATP-AlFx state (4.7 Å; Cong *et al*, 2010), the resolutions of the rest of the four states are assessed to be in the 10.5–13.9 Å resolution range based on the

0.5 cutoff for the Fourier Shell Correlation (Saxton and Baumeister, 1982; Harauz and van Heel, 1986).

Map segmentation and visualization were done with CHIMERA (http://www.cgl.ucsf.edu/chimera/; Pettersen *et al*, 2004).

Validation of the existence of the one-ring closed conformation in TRiC–ADP-AlFx data set

The existence of the one-ring closed asymmetric conformation induced by ATP hydrolysis is validated by our reference-free 2D image analysis and 3D reconstruction. First, the 2D image analysis of TRiC–ADP-AlFx particles depicts a unique end-on view in which all the subunits appear twisted (Supplementary Figure S1B), not seen in any of the other four states. If the two rings were in the same conformation, there would be no handedness in the end-on projection of TRiC as seen here. The twisted pattern is comparable to computed projections of the true bullet-shaped GroEL–Aacpn10–ADP complex (Chen *et al*, 2008), as well as a simulated asymmetric map (composed of a closed ring from TRiC–ATP-AlFx and an open ring from apo-TRiC). Moreover, our 3D reconstruction using *multirefine* in EMAN1 (Chen *et al*, 2006) indicates that the majority of TRiC particles ($\sim$65%) in this data set adopt the one-ring closed conformation (and were used in the reconstruction of the map shown in Figure 3A), while the remainder is in the conformation with both rings open (Supplementary Figure S1A and C), similar to the other open conformations of TRiC. The above analyses clearly confirm the existence of this asymmetric intermediate of TRiC in the ATP hydrolysis transition state (mimicked by ADP-AlFx).

Pseudo atomic model building by flexible fitting

To interpret the structural mechanism in more detail, a pseudo atomic model for each state was generated. We first built a homology model of the TRiC complex in the closed state (TRiC–ATP-AlFx). Since the current reconstructions were completed at relatively low resolution, we began with a homology model corresponding to the CCT2 subunit using thermosome (1A6D) as template and fit it as rigid body to all the subunits in the closed TRiC–ATP-AlFx map. In order to fit the closed-state model of the entire TRiC complex to each of the maps in different biochemical states, we used the real-space refinement/sampling program DireX (Schroder *et al*, 2007, 2010). DireX uses a geometrical sampling approach to flexibly fit a model into the density map in an iterative manner while ensuring correct stereochemistry and non-overlapping atoms. The model of the closed state was first placed into the density map of apo-TRiC using CHIMERA (Pettersen *et al*, 2004). Strong elastic restraints were used to avoid overfitting the density. The restraints were chosen between randomly chosen atoms that are within a distance range of 3–15 Å and that are separated by not $>$100 residues along the protein chain. The number of restraints was chosen as two times the number of atoms. The fitted model of apo-TRiC then served as the starting point for the refinements of other states. For the fitting, 500 optimization steps were performed with DireX, which took on average about 7 h on a single cpu (Intel Nehalem 2.93 GHz). In all refinements, a restrained grouped occupancy refinement was used, which adapted the contribution of the residues to the model density. This was done to account for reduced or missing density. This, however, adds only a small shift to the global position and orientation of the individual subunits and has almost no influence on the local structure. Finally, the models were subjected to minimization with CNS (Brunger, 2007). As shown in Supplementary Figure S3, these models fit to the corresponding density maps well particularly for equatorial and intermediate domains. Our models do not include some regions of the apical domain in several subunits, for example, in apo-TRiC, because the map in those regions was not very well resolved due to the dynamic nature of those subunits. However, such models are useful and simplified to represent the structural complexity and variations of TRiC in the ATPase cycle.

Accession codes

The density maps are deposited to EMDB (accession numbers EMD-1960, EMD-1961, EMD-1962, and EMD-1963) and the associated models are deposited to PDB (PDB IDs: 4A0O, 4A0V, 4A0W, and 4A13). They will be released upon publication.

Supplementary data

Supplementary data are available at *The EMBO Journal* Online (http://www.embojournal.org).

Acknowledgements

We thank Dr John F Flanagan IV for the help in composing the map unwrapping tools. This research is supported by grants from NIH through the Common Fund (PN1EY016525), NIGMS (GMR01-074074), and National Center for Research Resources (P41RR002250).

Author contributions: YC, JF, and WC designed research; ASM and SR prepared the specimen and defined the biochemical conditions for attaining different states; YC and JJ collected the cryo-EM data; YC carried out all the image processing and map analysis with the advice of SJL and MFS, and BM involved in the data preprocessing; YC and GFS built the models; YC, MTD, and WC generated the movies; YC, ASM, MFS, JF, and WC interpreted the structures; YC, GFS, ASM, MFS, SR, ML, SJL, JF, and WC wrote the paper.

Conflict of interest

The authors declare that they have no conflict of interest.

References

Archibald JM, Blouin C, Doolittle WF (2001) Gene duplication and the evolution of group II chaperonins: implications for structure and function. *J Struct Biol* **135:** 157–169

Bigotti MG, Clarke AR (2005) Cooperativity in the thermosome. *J Mol Biol* **348:** 13–26

Booth CR, Meyer AS, Cong Y, Topf M, Sali A, Ludtke SJ, Chiu W, Frydman J (2008) Mechanism of lid closure in the eukaryotic chaperonin TRiC/CCT. *Nat Struct Mol Biol* **15:** 746–753

Braig K, Otwinowski Z, Hegde R, Boisvert DC, Joachimiak A, Horwich AL, Sigler PB (1994) The crystal structure of the bacterial chaperonin GroEL at 2.8 A. *Nature* **371:** 578–586

Brunger AT (2007) Version 1.2 of the crystallography and NMR system. *Nat Protoc* **2:** 2728–2733

Bukau B, Horwich AL (1998) The Hsp70 and Hsp60 chaperone machines. *Cell* **92:** 351–366

Chen DH, Luke K, Zhang J, Chiu W, Wittung-Stafshede P (2008) Location and flexibility of the unique C-terminal tail of Aquifex aeolicus co-chaperonin protein 10 as derived by cryo-electron microscopy and biophysical techniques. *J Mol Biol* **381:** 707–717

Chen DH, Song JL, Chuang DT, Chiu W, Ludtke SJ (2006) An expanded conformation of single-ring GroEL-GroES complex encapsulates an 86 kDa substrate. *Structure* **14:** 1711–1722

Chen X, Sullivan DS, Huffaker TC (1994) Two yeast genes with similarity to TCP-1 are required for microtubule and actin function *in vivo*. *Proc Natl Acad Sci USA* **91:** 9111–9115

Clare DK, Stagg S, Quispe J, Farr GW, Horwich AL, Saibil HR (2008) Multiple states of a nucleotide-bound group 2 chaperonin. *Structure* **16:** 528–534

Cong Y, Baker ML, Jakana J, Woolford D, Miller EJ, Reissmann S, Kumar RN, Redding-Johanson AM, Batth TS, Mukhopadhyay A, Ludtke SJ, Frydman J, Chiu W (2010) 4.0-Å resolution cryo-EM structure of the mammalian chaperonin TRiC/CCT reveals its unique subunit arrangement. *Proc Natl Acad Sci USA* **107:** 4967–4972

Cong Y, Jiang W, Birmanns S, Zhou ZH, Chiu W, Wriggers W (2005) Fast rotational matching of single-particle images. *J Struct Biol* **152:** 104–112

Cong Y, Kovacs JA, Wriggers W (2003) 2D fast rotational matching for image processing of biophysical data. *J Struct Biol* **144:** 51–60

Cong Y, Ludtke SJ (2010) Single particle analysis at high resolution. *Methods Enzymol* **482:** 211–235

Cong Y, Zhang Q, Woolford D, Schweikardt T, Khant H, Dougherty M, Ludtke SJ, Chiu W, Decker H (2009) Structural mechanism of

SDS-induced enzyme activity of scorpion hemocyanin revealed by electron cryomicroscopy. *Structure* **17:** 749–758

Dekker C, Roe SM, McCormack EA, Beuron F, Pearl LH, Willison KR (2011) The crystal structure of yeast CCT reveals intrinsic asymmetry of eukaryotic cytosolic chaperonins. *EMBO J* **30:** 3078–3090

Ditzel L, Lowe J, Stock D, Stetter KO, Huber H, Huber R, Steinbacher S (1998) Crystal structure of the thermosome, the archaeal chaperonin and homolog of CCT. *Cell* **93:** 125–138

Dobson CM (2004) Principles of protein folding, misfolding and aggregation. *Semin Cell Dev Biol* **15:** 3–16

Douglas NR, Reissmann S, Zhang J, Chen B, Jakana J, Kumar R, Chiu W, Frydman J (2011) Dual action of ATP hydrolysis couples lid closure to substrate release into the group II chaperonin chamber. *Cell* **144:** 240–252

Feldman DE, Spiess C, Howard DE, Frydman J (2003) Tumorigenic mutations in VHL disrupt folding *in vivo* by interfering with chaperonin binding. *Mol Cell* **12:** 1213–1224

Ferreyra RG, Frydman J (2000) Purification of the cytosolic chaperonin TRiC from bovine testis. *Methods Mol Biol* **140:** 153–160

Frydman J (2001) Folding of newly translated proteins *in vivo*: the role of molecular chaperones. *Annu Rev Biochem* **70:** 603–647

Frydman J, Nimmesgern E, Erdjument-Bromage H, Wall JS, Tempst P, Hartl FU (1992) Function in protein folding of TRiC, a cytosolic ring complex containing TCP-1 and structurally related subunits. *EMBO J* **11:** 4767–4778

Gregersen N, Bross P, Jorgensen MM, Corydon TJ, Andresen BS (2000) Defective folding and rapid degradation of mutant proteins is a common disease mechanism in genetic disorders. *J Inherit Metab Dis* **23:** 441–447

Gutsche I, Holzinger J, Rossle M, Heumann H, Baumeister W, May RP (2000) Conformational rearrangements of an archaeal chaperonin upon ATPase cycling. *Curr Biol* **10:** 405–408

Harauz G, van Heel M (1986) Exact filters for general geometry three dimensional reconstruction. *Optik* **73:** 146–156

Hartl FU, Hayer-Hartl M (2002) Molecular chaperones in the cytosol: from nascent chain to folded protein. *Science* **295:** 1852–1858

Horst M, Oppliger W, Feifel B, Schatz G, Glick BS (1996) The mitochondrial protein import motor: dissociation of mitochondrial hsp70 from its membrane anchor requires ATP binding rather than ATP hydrolysis. *Protein Sci* **5:** 759–767

Huo Y, Hu Z, Zhang K, Wang L, Zhai Y, Zhou Q, Lander G, Zhu J, He Y, Pang X, Xu W, Bartlam M, Dong Z, Sun F (2010) Crystal structure of group II chaperonin in the open state. *Structure* **18:** 1270–1279

Kafri G, Horovitz A (2003) Transient kinetic analysis of ATP-induced allosteric transitions in the eukaryotic chaperonin containing TCP-1. *J Mol Biol* **326:** 981–987

Kafri G, Willison KR, Horovitz A (2001) Nested allosteric interactions in the cytoplasmic chaperonin containing TCP-1. *Protein Sci* **10:** 445–449

Kusmierczyk AR, Martin J (2003a) Nested cooperativity and salt dependence of the ATPase activity of the archaeal chaperonin Mm-cpn. *FEBS Lett* **547:** 201–204

Kusmierczyk AR, Martin J (2003b) Nucleotide-dependent protein folding in the type II chaperonin from the mesophilic archaeon Methanococcus maripaludis. *Biochem J* **371:** 669–673

Llorca O, Martin-Benito J, Grantham J, Ritco-Vonsovici M, Willison KR, Carrascosa JL, Valpuesta JM (2001) The 'sequential allosteric ring' mechanism in the eukaryotic chaperonin-assisted folding of actin and tubulin. *EMBO J* **20:** 4065–4075

Llorca O, Smyth MG, Carrascosa JL, Willison KR, Radermacher M, Steinbacher S, Valpuesta JM (1999) 3D reconstruction of the ATP-bound form of CCT reveals the asymmetric folding conformation of a type II chaperonin. *Nat Struct Biol* **6:** 639–642

Ludtke SJ, Baker ML, Chen DH, Song JL, Chuang DT, Chiu W (2008) *De novo* backbone trace of GroEL from single particle electron cryomicroscopy. *Structure* **16:** 441–448

Ludtke SJ, Baldwin PR, Chiu W (1999) EMAN: semiautomated software for high-resolution single-particle reconstructions. *J Struct Biol* **128:** 82–97

Ludtke SJ, Jakana J, Song JL, Chuang DT, Chiu W (2001) A 11.5 A single particle reconstruction of GroEL using EMAN. *J Mol Biol* **314:** 253–262

Ma J, Sigler PB, Xu Z, Karplus M (2000) A dynamic model for the allosteric mechanism of GroEL. *J Mol Biol* **302:** 303–313

Melki R, Batelier G, Soulie S, Williams Jr RC (1997) Cytoplasmic chaperonin containing TCP-1: structural and functional characterization. *Biochemistry* **36:** 5817–5826

Meyer AS, Gillespie JR, Walther D, Millet IS, Doniach S, Frydman J (2003) Closing the folding chamber of the eukaryotic chaperonin requires the transition state of ATP hydrolysis. *Cell* **113:** 369–381

Munoz IG, Yebenes H, Zhou M, Mesa P, Serna M, Park AY, Bragado-Nilsson E, Beloso A, de Carcer G, Malumbres M, Robinson CV, Valpuesta JM, Montoya G (2011) Crystal structure of the open conformation of the mammalian chaperonin CCT in complex with tubulin. *Nat Struct Mol Biol* **18:** 14–19

Pereira JH, Ralston CY, Douglas NR, Meyer D, Knee KM, Goulet DR, King JA, Frydman J, Adams PD (2010) Crystal structures of a group II chaperonin reveal the open and closed states associated with the protein folding cycle. *J Biol Chem* **285:** 27958–27966

Pettersen EF, Goddard TD, Huang CC, Couch GS, Greenblatt DM, Meng EC, Ferrin TE (2004) UCSF Chimera–a visualization system for exploratory research and analysis. *J Comput Chem* **25:** 1605–1612

Reissmann S (2007) *Mechanism of action of group II chaperonins: impact of the built-in lid on the conformational cycle*. Ph.D. thesis, Department of Biological Sciences Stanford University, Stanford

Reissmann S, Parnot C, Booth CR, Chiu W, Frydman J (2007) Essential function of the built-in lid in the allosteric regulation of eukaryotic and archaeal chaperonins. *Nat Struct Mol Biol* **14:** 432–440

Rommelaere H, Van Troys M, Gao Y, Melki R, Cowan NJ, Vandekerckhove J, Ampe C (1993) Eukaryotic cytosolic chaperonin contains t-complex polypeptide 1 and seven related subunits. *Proc Natl Acad Sci USA* **90:** 11975–11979

Saxton WO, Baumeister W (1982) The correlation averaging of a regularly arranged bacterial cell envelope protein. *J Microsc* **127:** 127–138

Schroder GF, Brunger AT, Levitt M (2007) Combining efficient conformational sampling with a deformable elastic network model facilitates structure refinement at low resolution. *Structure* **15:** 1630–1641

Schroder GF, Levitt M, Brunger AT (2010) Super-resolution biomolecular crystallography with low-resolution data. *Nature* **464:** 1218–1222

Shomura Y, Yoshida T, Iizuka R, Maruyama T, Yohda M, Miki K (2004) Crystal structures of the group II chaperonin from Thermococcus strain KS-1: steric hindrance by the substituted amino acid, and inter-subunit rearrangement between two crystal forms. *J Mol Biol* **335:** 1265–1278

Southworth DR, Agard DA (2008) Species-dependent ensembles of conserved conformational states define the Hsp90 chaperone ATPase cycle. *Mol Cell* **32:** 631–640

Spiess C, Meyer AS, Reissmann S, Frydman J (2004) Mechanism of the eukaryotic chaperonin: protein folding in the chamber of secrets. *Trends Cell Biol* **14:** 598–604

Szpikowska BK, Swiderek KM, Sherman MA, Mas MT (1998) MgATP binding to the nucleotide-binding domains of the eukaryotic cytoplasmic chaperonin induces conformational changes in the putative substrate-binding domains. *Protein Sci* **7:** 1524–1530

Tang G, Peng L, Baldwin PR, Mann DS, Jiang W, Rees I, Ludtke SJ (2007) EMAN2: an extensible image processing suite for electron microscopy. *J Struct Biol* **157:** 38–46

Thulasiraman V, Yang CF, Frydman J (1999) *In vivo* newly translated polypeptides are sequestered in a protected folding environment. *EMBO J* **18:** 85–95

Tian G, Vainberg IE, Tap WD, Lewis SA, Cowan NJ (1995) Specificity in chaperonin-mediated protein folding. *Nature* **375:** 250–253

Tsutsumi S, Mollapour M, Graf C, Lee CT, Scroggins BT, Xu W, Haslerova L, Hessling M, Konstantinova AA, Trepel JB, Panaretou B, Buchner J, Mayer MP, Prodromou C, Neckers L (2009) Hsp90 charged-linker truncation reverses the functional consequences of weakened hydrophobic contacts in the N domain. *Nat Struct Mol Biol* **16:** 1141–1147

Xu Z, Horwich AL, Sigler PB (1997) The crystal structure of the asymmetric GroEL-GroES-(ADP)7 chaperonin complex. *Nature* **388:** 741–750

Yam AY, Xia Y, Lin HT, Burlingame A, Gerstein M, Frydman J (2008) Defining the TRiC/CCT interactome links chaperonin function to stabilization of newly made proteins with complex topologies. *Nat Struct Mol Biol* **15:** 1255–1262

Zhang J, Baker ML, Schroder GF, Douglas NR, Reissmann S, Jakana J, Dougherty M, Fu CJ, Levitt M, Ludtke SJ, Frydman J, Chiu W (2010) Mechanism of folding chamber closure in a group II chaperonin. *Nature* **463:** 379–383

Zhang J, Ma B, Dimaio F, Douglas NR, Joachimiak LA, Baker D, Frydman J, Levitt M, Chiu W (2011) Cryo-EM structure of a group II chaperonin in the prehydrolysis ATP-bound state leading to lid closure. *Structure* **19:** 633–639

